EPJ Web of Conferences **182**, 02102 (2018) https://doi.org/10.1051/epjconf/201818202102
ICNFP 2017

Latest results on diffraction at HERA

Mariusz Przybycien[1,a] (on behalf of the H1 and ZEUS Collaborations)

[1] *AGH University of Science and Technology, Faculty of Physics and Applied Computer Science Al. Mickiewicza 30, 30-059 Cracow, Poland*

Abstract. Recent results on diffraction from the H1 and ZEUS experiments at HERA are presented. Measurement of open charm production in diffractive DIS has been performed by the H1 experiment using the event topology, given by $ep \to eXY$, where the system X, containing at least one $D^*(2010)$ meson, is separated from a leading low-mass proton dissociative system Y by a large rapidity gap. The photoproduction of isolated photons is measured using diffractive events recorded by the ZEUS experiment. Cross sections are evaluated in the photon transverse-energy and pseudorapidity ranges $5 < E_{\mathrm{T}}^{\gamma} < 15$ GeV and $-0.7 < \eta_{\gamma} < 0.9$, inclusively and with a jet with transverse-energy and pseudorapidity in the ranges $4 < E_{\mathrm{T}}^{\mathrm{jet}} < 35$ GeV and $-1.5 < \eta_{\mathrm{jet}} < 1.8$. The exclusive deep inelastic electroproduction and photoproduction of $\Psi(2S)$ and $J/\Psi(1S)$ mesons has been also studied by ZEUS. The cross-section ratio $\sigma(\Psi(2S))/\sigma(J/\Psi(1S))$ has been measured as a function of Q^2, W and t. The results are compared to several predictions of QCD-inspired models, providing tests of the models in a region of soft to hard diffraction.

1 Introduction

Diffractive interactions are a distinctive class of hadronic interactions in which the scattering of the incoming particle is mediated by an exchanged object carrying vacuum quantum numbers, commonly referred to as the Pomeron [1, 2]. At the HERA ep collider, diffractive processes have been studied both in photoproduction and in deep inelastic scattering (DIS), photoproduction processes being those in which the exchanged photon is quasireal. Diffractive processes of this kind are typically characterised by a forward nucleon or nucleonic state that is separated by a gap in rapidity from the hadronic final state produced in the central region of the event. The physical nature of the Pomeron is not fully established within quantum chromodynamics (QCD), and a number of models have been proposed. In an approach originated by Ingelman and Schlein [3], the Pomeron is taken to be a hadron-like object that contains quarks and gluons. The Pomeron parton density functions (PDFs) can be evaluated from fits to diffractive DIS (DDIS) data [4]. In an alternative approach [5], the Pomeron is equivalent to the exchange of two gluons.

The standard DIS kinematics in ep collisions is described in terms of the invariants:

$$s = (k + P)^2, \qquad Q^2 = -q^2, \qquad y = \frac{q \cdot P}{k \cdot P}, \qquad W = (q + P)^2, \qquad x = \frac{Q^2}{2q \cdot P}$$

[a] e-mail: Mariusz.Przybycien@agh.edu.pl

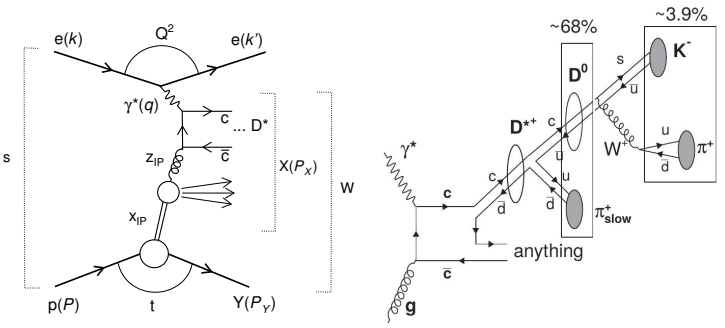

Figure 1. (left) The LO diagram for open charm production in DDIS at HERA in the picture of collinear and proton vertex factorisation. Kinematic variables describing the DDIS processes in general as well as particles four-momenta are also indicated. (right) $D^\star$ production in boson-gluon fusion process with subsequent decays in the 'golden channel' as described in the text.

where the four-vectors are indicated in Fig. 1(left). Here s is the square of the total centre-of-mass energy of the collision, Q^2 the photon virtuality, y the scattered electron inelasticity, W^2 the centre-of-mass energy squared of the $\gamma^\star p$ system and x the Bjorken scaling variable. Given the two hadronic systems X and Y, separated by a large rapidity gap, diffractive kinematic variables are defined as follows:

$$M_X^2 = (P_X)^2, \quad M_Y^2 = (P_Y)^2, \quad t = (P - P_Y)^2, \quad x_{I\!P} = \frac{q \cdot (P - P_Y)}{q \cdot P}, \quad z_{I\!P} = \frac{\hat{s} + Q^2}{M_X^2 + Q^2}$$

In inclusive DDIS, where M_X and M_Y are the invariant masses of the systems X and Y, respectively, t is the squared four-momentum transfer at the proton vertex and $x_{I\!P}$ the fraction of the proton's longitudinal momentum taken by the Pomeron. $z_{I\!P}$ is the fraction of the Pomeron momentum that takes part in the hard interaction, and $\hat{s}$ denotes the centre-of-mass energy squared of the hard process.

2 Recent measurements at HERA

Measurements of diffractive processes are presented below based on data collected by the H1 and ZEUS experiments at the HERA Collider, where beams of electrons/positrons of energy 27.5 GeV were collided with protons of energy 920 GeV. This corresponds to the energy available in the centre-of-mass system equal to $\sqrt{s} = 318$ GeV.

The H1 Colaboration has performed a measurement of $D^\star$ production in DDIS [6]. The process is schematically shown in Fig. 1(left). The $D^\star$ meson originates from the fragmentation of a charm quark, which is produced at HERA energies mainly via the boson-gluon fusion ($\gamma^\star g \to c\bar{c}$) process. Hence, the gluon content of the Pomeron can be accessed directly, and allows the collinear factorisation to be tested. The detection of $D^\star$ mesons is based on the full reconstruction of its decay products in the 'golden channel'

$$D^{\star+} \to D^0 \pi^+_{slow} \to (K^-\pi^+)\pi^+_{slow} \quad (+C.C.)$$

with subsequent branching ratios as indicated in Fig. 1(right). The cross sections are measured in the fiducial range defined by DIS phase space $5 < Q^2 < 100$ GeV^2, $0.02 < y < 0.65$, $D^\star$ kinematics $p_{t,D^\star} > 1.5$ GeV, $|\eta_{D^\star}| < 1.5$ and diffractive phase space $x_{I\!P} < 0.03$, $M_Y > 1.6$ GeV and $|t| < 1$ GeV^2.

Figure 2(left) shows the differential cross sections as functions of kinematic variables $\log_{10}(x_{I\!P})$ and $z_{I\!P}^{\rm obs}$. The shape of $\mathrm{d}\sigma/\mathrm{d}\log_{10}(x_{I\!P})$ is satisfactorily described by the NLO QCD prediction by HVQDIS [7, 8] given the large relative uncertainties at low $x_{I\!P}$ values. The shape of $\mathrm{d}\sigma/\mathrm{d}z_{I\!P}^{\rm obs}$ is not described as well by the prediction, however the experimental uncertainties at low $z_{I\!P}^{\rm obs}$ are sizeable.

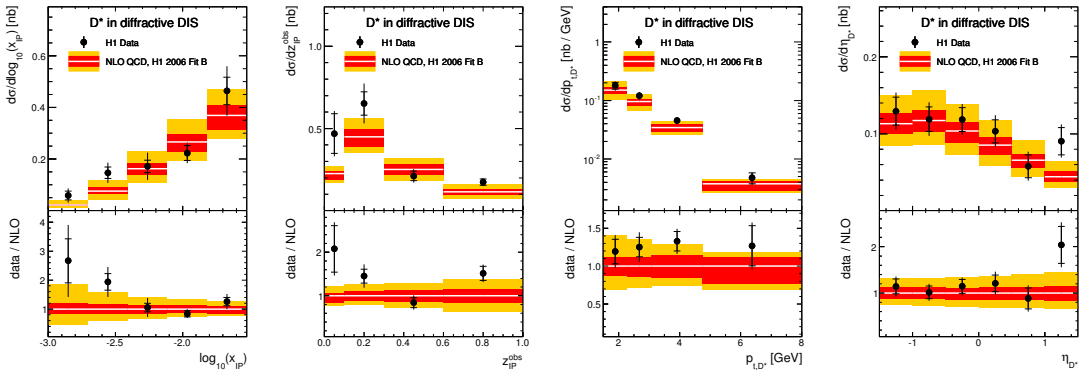

Figure 2. Bin averaged single-differential $D^\star$ cross sections as a function of the variables $\log(x_{I\!P})$, $z_{I\!P}^{\rm obs}$, $p_{t,D^\star}$ and $\eta_{D^\star}$. Data are shown as dots, where the inner error bars indicate statistical uncertainties and the outer error bars represent the statistical and the full set of systematic uncertainties added in quadrature. The central NLO QCD prediction by HVQDIS is shown as a white line inside the coloured bands. The inner band represents the DPDF and fragmentation uncertainties added in quadrature. The outer band represents DPDF, fragmentation, charm mass, factorisation and renormalisation scale uncertainties added in quadrature.

The differential cross sections as functions of $D^\star$ transverse momentum $p_{t,D^\star}$ and pseudorapidity $\eta_{D^\star}$ are shown in Fig. 2(right). The shapes of $\mathrm{d}\sigma/\mathrm{d}p_{t,D^\star}$ and $\mathrm{d}\sigma/\mathrm{d}\eta_{D^\star}$ are well described by the theory. For $\eta_{D^\star} > 1$, however, the theory predicts a value which underestimates the data by about 50% with a large uncertainty. There is an indication of a similar effect in the corresponding non-diffractive $D^\star$ cross section measurement [9].

The measured diffractive cross sections together with the non-diffractive one published in Ref. [9] can be used to calculate the diffractive fraction $R_D = \sigma_{D^\star}^{\rm diff}/\sigma_{D^\star}^{\rm non-diff}$. The differential fractions $R_D(y)$, $R_D(Q^2)$, $R_D(p_{t,D^\star})$ and $R_D(\eta_{D^\star})$ are shown in Fig. 3. Within uncertainties the data do not provide strong evidence for kinematic dependencies of R_D on Q^2 or y, while at the same time they are also consistent with the kinematic dependencies predicted by theory. The diffractive fraction decreases

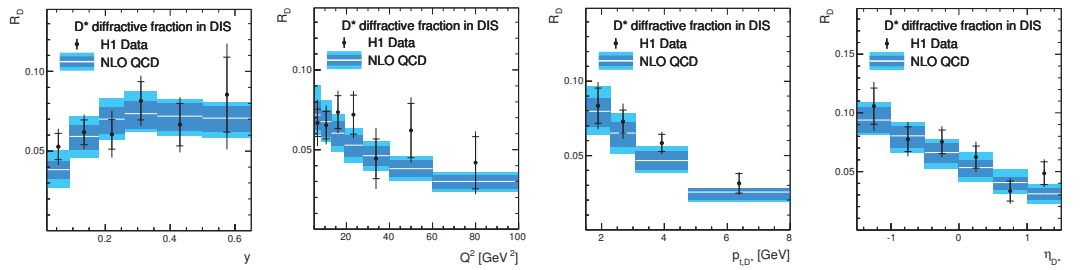

Figure 3. The diffractive fraction, R_D, measured as a ratio of bin averaged diffractive to non-diffractive $D^\star$ production single differential cross sections in deep inelastic scattering as a function of y, Q^2, $p_{t,D^\star}$ and $\eta_{D^\star}$. The data ratios are represented with dots, where the inner error bars indicate statistical uncertainties and the outer error bars represent the statistical and systematic uncertainties added in quadrature. The central NLO QCD prediction of R_D by HVQDIS is shown as a white line inside the coloured bands. The inner band represents DPDF uncertainty. The outer band represents effect of the DPDF uncertainty and simultaneous variations of scales, charm mass and fragmentation settings in the diffractive and non-diffractive calculations added in quadrature.

from 8% to 3% with $p_{t,D^\star}$ increasing. The measured dependence of the diffractive fraction on $\eta_{D^\star}$ decreases from 10% to about 5% for the highest $\eta_{D^\star}$ values. These shapes are well reproduced by the NLO QCD predictions from HVQDIS within the uncertainties. The shapes can be qualitatively understood as follows. Due to the high energy of the leading proton in diffraction ($x_{I\!P} < 0.03$) the system X is produced with low masses M_X. Less energy is available from the proton side to produce the hard system containing the $D^\star$ meson as compared to the non-diffractive case. Similarly, the fraction is suppressed for small y, i.e. for small energy of the exchanged virtual photon. The Q^2 dependence of R_D can be explained by the fact that at high Q^2 (higher x) the diffractive cross section is suppressed due to a limited $x_{I\!P}$ range. Likewise, due to the lack of energy, the events with higher $p_{t,D^\star}$ can be expected to be suppressed in diffraction. The diffractive fraction as a function of $\eta_{D^\star}$ indicates that in diffraction the hard system tends to be produced backwards, due to the kinematics constrained by the presence of a large rapidity gap, or equivalently the $x_{I\!P} < 0.03$ condition.

Diffractive photoproduction of isolated photons has been studied by ZEUS in Ref. [10]. The photon–Pomeron interaction can take place through processes in which the photon or Pomeron acts as a source of quarks and gluons, which then take part in the QCD scatter (resolved processes) and processes in which the photon or Pomeron interacts as a whole (direct processes). There are thus in principle four different types of process that may be experimentally studied: a direct or resolved photon interacting with a direct or resolved Pomeron. Examples of these processes are illustrated in Fig. 4. Direct Pomeron processes are not included in the Ingelman–Schlein model [3], but are taken into account in other approaches [11]. Within the Ingelman–Schlein framework, it is normally assumed that a Pomeron with a universal set of PDFs is emitted, making allowance for QCD evolution effects. In the H1 DIS analysis [4], the results of which are used here, the Pomeron PDFs are dominated by gluons in most regions of parameter space, but a significant quark content is also present. If the factorisation hypothesis holds, the same parton structure would be valid both in direct photoproduction processes and in DIS, although in resolved photon processes, absorptive effects may be present [12]. Several studies of diffractive dijet events in photoproduction and DIS have been carried out at HERA. In the present measurement of diffractive events in which a hard isolated "prompt" photon is detected in the central region of the ZEUS detector, it may be accompanied by one or more jets. Such processes, while rare, are interesting for a number of reasons. The prompt photon must originate from a charged parton, and its observation therefore demonstrates the presence either of a quark in the Pomeron or of higher-order processes in which both the Pomeron and the incident photon couple to quarks. This contrasts with diffractive dijet production, which is mainly sensitive to the gluon content of the Pomeron. Hard photons are also produced in fragmentation processes in which a photon is radiated within a jet. Such processes can be suppressed by requiring the observed hard photon to be isolated from other particles in the event.

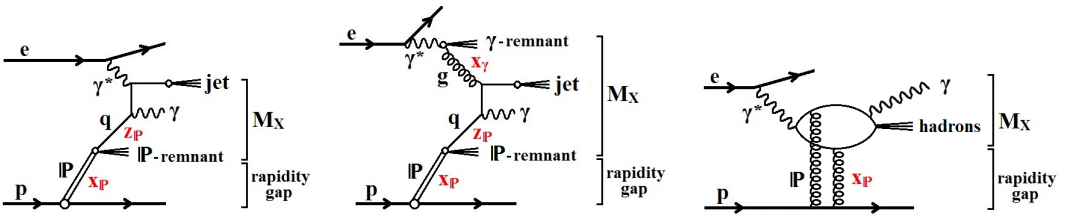

Figure 4. Examples of diagrams for the diffractive production of a prompt photon and a jet in ep scattering from (left) direct and (middle) resolved photons, interacting with a resolved Pomeron. (right) Example of an interaction between a direct photon and a direct Pomeron. The meaning of variables is similar to Fig. 1(left).

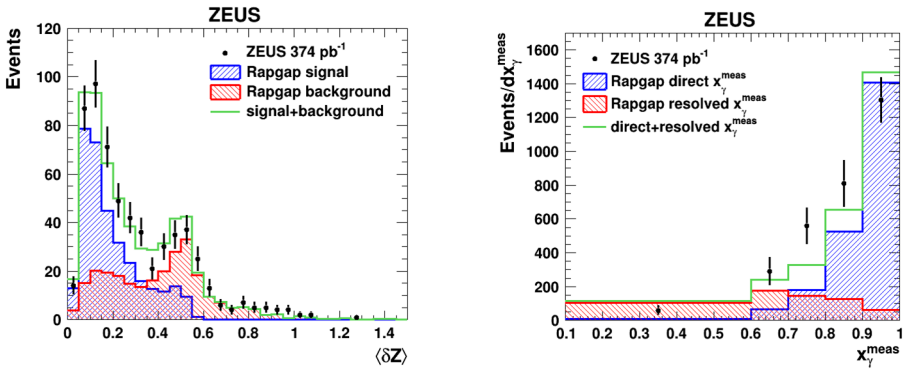

Figure 5. (left) Distribution of δZ for selected diffractive events with a photon candidate and at least one jet. The error bars denote the statistical uncertainties on the data, which are compared to the fitted signal and background components from the MC. The unit of measurement of δZ is the width of one BEMC cell. (right) Events with a photon and at least one jet as a function of $x_\gamma^{\rm meas}$, compared to a normalised 70:30 mixture of direct:resolved photon Rapgap events without reweighting.

The diffractive photoproduction of isolated photons, with and without at least one accompanying jet, has been measured in a kinematic region defined in the laboratory frame by: $Q^2 < 1$ GeV^2, $0.2 < y < 0.7$, $-0.7 < \eta_\gamma < 0.9$, $5 < E_{\rm T}^\gamma < 15$ GeV, $4 < E_{\rm T}^{\rm jet} < 35$ GeV and $-1.5 < \eta_{\rm jet} < 1.8$. The diffractive requirement was $\eta_{\rm max} < 2.5$ and $x_{I\!P} < 0.03$. Photon isolation was imposed by requiring that the photon had at least 90% of the energy of the reconstructed jet of which it formed a part. In order to additionaly remove background events in which one or more neutral mesons, such as π^0 and η, have decayed to photons, a template fit has been performed of expected from the Rapgap Monte Carlo [13] signal and background distributions as a function of the quantity

$$\langle \delta Z \rangle = \sum_i E_i |Z_i - Z_{\rm cluster}| / (w_{\rm cell} \sum_i E_i)$$

where Z_i is the Z position of the centre of the i-th cell, $Z_{\rm cluster}$ is the energy-weighted centroid of the EFO (Energy Flow Object - a reconstructed object in the ZEUS detector) cluster, $w_{\rm cell}$ is the width of the cell in the Z direction, and E_i is the energy recorded in the cell. The sum runs over all BEMC (Barrel Electromagnetic Calorimeter) cells in the EFO cluster. The results of the fit are shown in Fig. 5(left), and are used to statistically subtract the background for each measured cross section.

In direct photon processes, the incoming virtual photon is absorbed by a quark from the target particle, here a Pomeron, while in resolved photon processes, the virtual photon's hadronic structure provides a quark or gluon that interacts with a quark or gluon from the Pomeron. These two classes of process, which are unambiguously defined only at the leading order (LO) of QCD, may be partially distinguished in events containing a high-$E_{\rm T}$ photon and a jet by means of the quantity

$$x_\gamma^{\rm meas} = \frac{E^\gamma + E^{\rm jet} - p_Z^\gamma - p_Z^{\rm jet}}{E^{\rm all} - p_Z^{\rm all}}$$

which measures the fraction of the incoming photon energy that is given to the outgoing photon and jet. The quantities E^γ and $E^{\rm jet}$ denote the energies of the outgoing photon and the jet, respectively, and p_Z denotes the corresponding longitudinal momenta. The suffix "all" refers to all objects that are measured in the detector or, in the case of simulations at the hadron level, all final-state particles except for the scattered beam electron and the outgoing proton. Events with a detected final-state

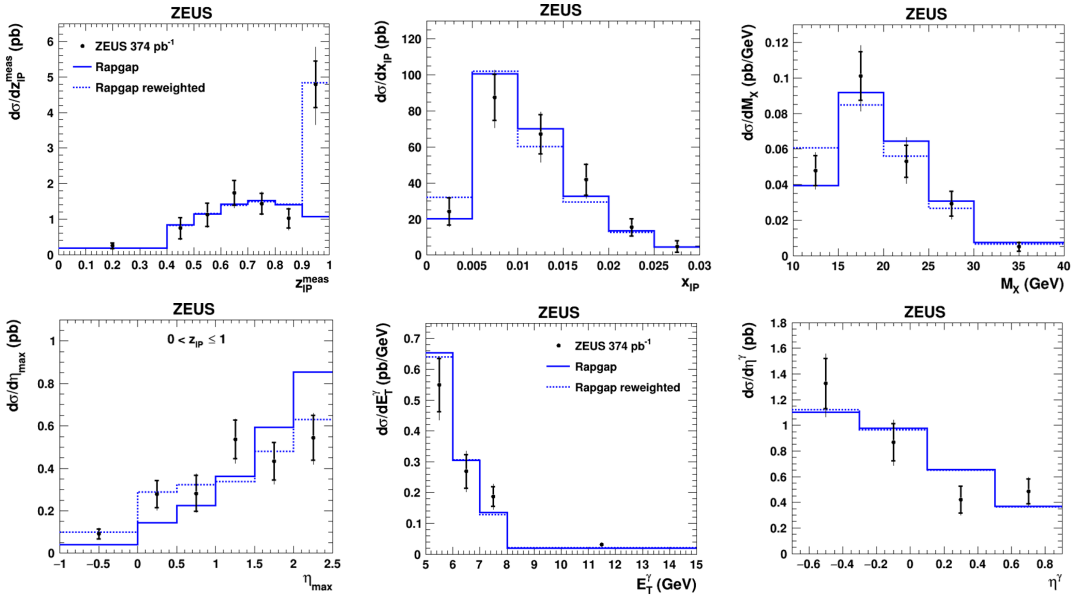

Figure 6. (left column) Differential cross section for isolated photon production accompanied by at least one jet, as a function of $z_{I\!P}^{\rm meas}$ and $\eta_{\rm max}$. (middle and right) Differential cross sections for inclusive isolated photon production as functions of $x_{I\!P}$, M_X, $E_{\rm T}^{\gamma}$ and η_{γ}. The inner error bars denote statistical uncertainties; the outer denote statistical with systematic uncertainties combined in quadrature. The Rapgap predictions are normalised to the data.

electron are excluded from this analysis. At LO, $x_{\gamma}^{\rm meas} = 1$ for direct photon events, while resolved photon events can have any value in the range $(0, 1)$. Direct photon events at higher order can have $x_{\gamma}^{\rm meas}$ less than unity, but the presence of the LO processes generates a prominent peak in the observed cross section at high values of $x_{\gamma}^{\rm meas}$. The distribution of events in $x_{\gamma}^{\rm meas}$ after final selection is shown in Fig. 5(right). A 70 : 30 mixture of direct:resolved photon events generated with Rapgap MC gives a reasonable description of the data and was employed in the analysis.

Differential cross sections are presented in terms of the transverse energy and pseudorapidity of the prompt photon and the jet, and of a number of variables that describe the kinematics of the diffractively produced system, in particular the fraction of the Pomeron energy given to the prompt photon and the jet, $z_{I\!P}$. Selected measurements are shown in Fig. 6. With the exception of $\eta_{\rm max}$ and $z_{I\!P}$, the distributions in all the variables are well described in shape by the standard Rapgap model over the whole $z_{I\!P}$ range and in the ranges $z_{I\!P} < 0.9$ and $z_{I\!P} > 0.9$ separately (not shown in the plots). For $z_{I\!P} > 0.9$, there is evidence for an excess in the data above the nominal Rapgap prediction. This excess indicates the presence of a direct Pomeron interaction, and is observed predominantly in the direct photon channel.

A measurement of the ratio of the cross sections for the reactions $\gamma^{\star} p \rightarrow \psi(2S) + Y$ and $\gamma^{\star} p \rightarrow J/\psi(1S) + Y$, where Y denotes either a proton or a low mass proton dissociative system has been performed by the ZEUS experiment [14]. The $\psi(2S)$ and the $J/\psi(1S)$ mesons have the same quark content, but different radial distributions of the wave functions, and their mass difference is small compared to the HERA centre-of-mass energy. Therefore this measurement allows QCD predictions of the wave function dependence of the $c\bar{c}$-proton cross section to be tested. A suppression of the $\psi(2S)$ cross section relative to the $J/\psi(1S)$ is expected, as the $\psi(2S)$ wave function has a radial node close to the typical transverse separation of the virtual $c\bar{c}$ pair.

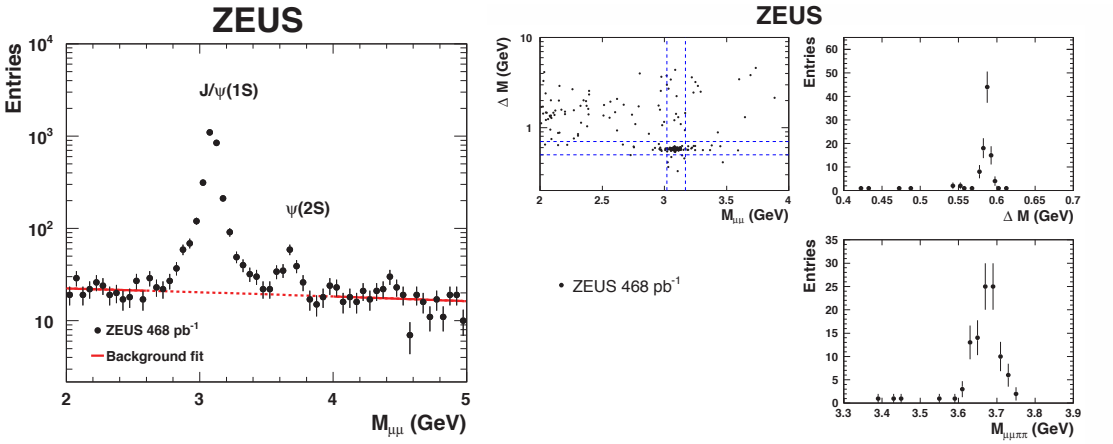

Figure 7. (left) Two-muon invariant mass distribution for exclusive dimuon events. (right) Selection of events with exclusive production of $\psi(2S)$ meson decaying into $\pi\pi\mu\mu$ system.

The ratio of the cross sections $\sigma(ep \to e\psi(2S)Y)/\sigma(ep \to eJ/\psi(1S)Y)$ has been measured in the kinematic range of $5 < Q^2 < 80\,\mathrm{GeV}^2$, $30 < W < 210\,\mathrm{GeV}$ and $|t| < 1\,\mathrm{GeV}^2$ using data corresponding to the luminosity of 468 pb^{-1}. An additional sample of 114 pb^{-1} was used to extend the measurement to the range $2 < Q^2 < 5\,\mathrm{GeV}^2$. Events were required to have no activity in the central ZEUS detector in addition to signals from the scattered electron and the decay products of the $\psi(2S)$ or $J/\psi(1S)$. The decay channels used were $J/\psi(1S) \to \mu^+\mu^-$, $\psi(2S) \to \mu^+\mu^-$ and $\psi(2S) \to J/\psi(1S)\pi^+\pi^-$ with the subsequent decay $J/\psi(1S) \to \mu^+\mu^-$.

The $\mu^+\mu^-$ mass distribution for the selected events in dimuon decay channels is shown in Fig. 7(left). Clear $J/\psi(1S)$ and $\psi(2s)$ peaks and no other significant peaks are observed. The background was fit by straight line in the side-bands of the signals. Selection of $\psi(2S)$ in the decay channel to $\pi^+\pi^-\mu^+\mu^-$ is based on the scatter plot of $\Delta M = M_{\mu\mu\pi\pi} - M_{\mu\mu}$ versus $M_{\mu\mu}$ shown in Fig. 7(right) together with distributions of the ΔM and $M_{\mu\mu\pi\pi}$ for $3.02 < M_{\mu\mu} < 3.17$ GeV. The ΔM distribution

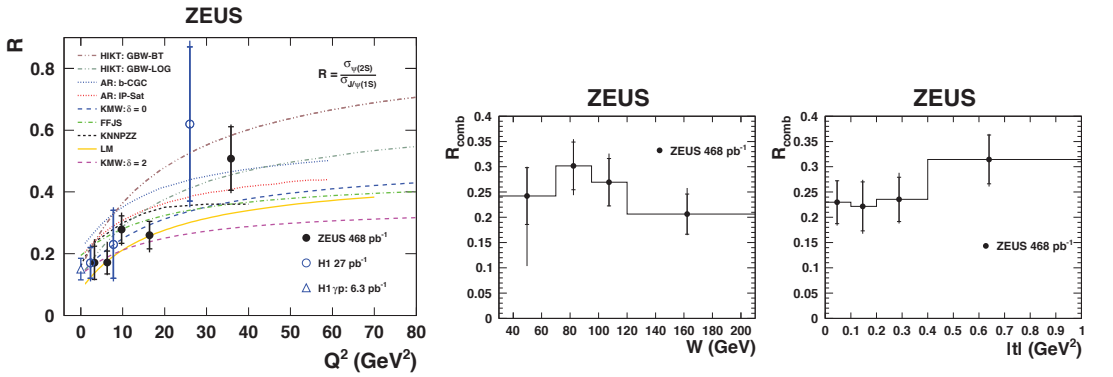

Figure 8. Cross section ratio $\sigma_{\psi(2S)}/\sigma_{J/\psi(1S)}$ for the combined $\psi(2S)$ decay modes as a function of Q^2 compared to previous H1 results and several model predictions (left), W (middle) and $|t|$ (right). The references to the H1 measurements and theory predictions one can find in [14].

show a narrow peak at the nominal $\psi(2S) - J/\psi(1S)$ mass difference. Simultaneous cuts on ΔM and $M_{\mu\mu}$ as shown by the dashed lines in the scatter plot were used to select the $\psi(2S) \to \mu\mu\pi\pi$ events.

The combined cross section ratio was obtained using the with the statistical uncertainties weighted average of the cross sections determined for the two $\psi(2S)$ decay channels. The measured ratios are shown in Fig. 8 as a function of Q^2, W and $|t|$. The data contain a background of charmonium production with diffractive masses $M_Y \lesssim 4$ GeV. Assuming that the cross section ratio does no vary with M_Y, the results are not affected by the proton dissociation background. The ratios as a function of W and $|t|$ are compatible with a constant. For the Q^2 dependence, a positive slope is observed. The data are in good agreement with the H1 measurements as well as with most of theory predictions shown.

3 Summary

Recent results on diffraction from the H1 and ZEUS experiments have been presented. For more details and in depth discussion of the measurements the reader is referred to the original publications.

References

[1] A. Donnachie, P.V. Landshoff, *Total cross-sections*, Phys. Lett. **B296** (1992) 227, [hep-ph/9209205].

[2] E. Feinberg, I. Pomeranchuk, *High energy inelastic diffraction phenomena*, Suppl. Nuovo Cimento 3 (1956) 652.

[3] G. Ingelman and P. Schlein, *Jet Structure in High Mass Diffractive Scattering*, Phys. Lett. **B152** (1985) 256.

[4] H1 Collaboration, A. Aktas et al., *Measurement and QCD Analysis of the Diffractive Deep-Inelastic Scattering Cross Section at HERA*, Eur. Phys. J. **C48** (2006) 715, [hep-ex/0606004].

[5] J. Bartels, H. Lotter, M. Wuesthoff, *Quark-Antiquark Jets in DIS Diffractive Dissociation*, iPhys. Lett. **B379** (1996) 239, [hep-ph/9609239].

[6] H1 Collaboration, et al., *Measurement of D production in diffractive deep inelastic scattering at HERA*, Eur. Phys. J. **C77** (2017) 340, [hep-ex/1703.09476].

[7] B.W. Harris, J. Smith, *Heavy quark correlations in deep inelastic electroproduction*, Nucl. Phys. **B452** (1995) 109, [hep-ph/9503484].

[8] B.W. Harris, J. Smith, *Charm quark and $D^{\star\pm}$ cross-sections in deeply inelastic scattering at HERA*, Phys. Rev. **D57** (1998) 2806, [hep-ph/9706334].

[9] H1 Collaboration, F.D. Aaron et al., *Measurement of $D^{\star\pm}$ Meson Production and Determination of $F_2^{c\bar{c}}$ at low Q^2 in Deep-Inelastic Scattering at HERA*, Eur. Phys. J. **C71** (2011) 1769, Erratum: Eur. Phys. J. **C72** (2012) 2252, [hep-ph/1106.1028].

[10] ZEUS Collaboration, H. Abramowicz et al., *Studies of the diffractive photoproduction of isolated photons at HERA*, Phys. Rev. **D96** (2017) 032006, [hep-ex/1705.10251].

[11] B. Kniehl, H.-G. Kohrs and G. Kramer, *Diffractive photoproduction of jets with a direct pomeron coupling at HERA*, Z. Phys. **C65** (1995) 657, [hep-ph/9408340].

[12] A. Kaidalov, V. Khoze, A. Martin, and M. Ryskin, *Probabilities of rapidity gaps in high-energy interactions*, Eur. Phys. J. **C21** (2001) 521, [hep-ph/0105145].

[13] H. Jung, *Hard diffractive scattering in high-energy e p collisions and the Monte Carlo generator RAPGAP*, Comput.Phys.Commun. 86 (1995) 147-161, https://rapgap.hepforge.org/rapgap.pdf.

[14] ZEUS Collaboration, H. Abramowicz et al., *Measurement of the cross section ratio $\sigma_{\psi(2S))}/\sigma_{J/\psi(1S)}$ in deep inelastic ep scattering at HERA*, Nucl. Phys. **B909** (2016) 934-953, [hep-ex/1606.08652].